EUROPEAN JOURNAL OF PURE AND APPLIED MATHEMATICS
2025, Vol. 18, Issue 4, Article Number 6958
ISSN 1307-5543 – ejpam.com
Published by New York Business Global

Numerical Study of Nano-encapsulated Phase Change Materials on Non-Newtonian Nanofluid Flow over a Stretching Sheet

Leli Deswita[1,*], Syamsudhuha Syamsudhuha[1], Rustam Effendi[1], Asral Asral[2]

[1] *Department of Mathematics, Faculty of Mathematics and Science, Universitas Riau, 28293 Pekanbaru, Riau, Indonesia*
[2] *Department of Mechanical Engineering, Engineering Faculty, Universitas Riau, 28293 Pekanbaru, Riau, Indonesia*

Abstract. This study analyzes the hydrodynamic and thermal behavior of a power-law nanofluid containing nano-encapsulated phase change materials (NEPCMs) over a non-isothermal stretching sheet. The combined effects of non-Newtonian rheology and latent heat transport due to NEPCM inclusions are formulated through boundary-layer theory and the power-law constitutive relation. The resulting nonlinear similarity equations are solved numerically using the shooting technique with Runge–Kutta integration. Results indicate that embedding NEPCM particles within the power-law nanofluid significantly enhances heat transfer through latent heat absorption and release, though it also increases wall shear stress. Higher power-law indices suppress velocity and temperature distributions, mitigating this shear enhancement. These findings reveal a competing interaction between fluid rheology and the thermal storage capacity of NEPCMs. The study offers new insights into the coupled flow and heat transfer mechanisms of NEPCM-suspended power-law nanofluids, with relevance to advanced cooling, polymer processing, and energy storage applications.

2020 Mathematics Subject Classifications: 41A30, 76F12, 65M60, 65N12

Key Words and Phrases: Runge–Kutta method, NEPCM, phase change heat transfer, nanofluids, boundary layer

1. Introduction

The behavior of non-Newtonian fluids is integral to numerous natural processes and industrial applications due to their shear rate- and shear stress-dependent viscosity, which is a distinctive property of these fluids. This distinctive property of non-Newtonian fluids

*Corresponding author.
DOI: https://doi.org/10.29020/nybg.ejpam.v18i4.6958

Email addresses: leli.deswita@lecturer.unri.ac.id (L. Deswita), syamsudhuha@lecturer.unri.ac.id (S. Syamsudhuha), rustam@lecturer.unri.ac.id (R. Effendi), asral@lecturer.unri.ac.id (A. Asral)

has enabled their use in a variety of industrial and engineering contexts, including the manufacture of plastics, mining, transportation, aerodynamics, lubrication, and biological and natural systems such as bodily fluids and wet sand. Non-Newtonian fluids display a range of rheological behaviours, including shear thinning and shear thickening, which depend on the shear rate applied. Due to their intricate nature, these fluids cannot be described by a single constitutive equation. Consequently, numerous mathematical models have been proposed to characterise their behavior, with the power-law model being the most widely adopted for describing pseudoplastic and dilatant fluids.

Extensive research has been conducted on power-law fluid flows, highlighting their multifaceted properties and applications. Cobble [1] analyzed the flow of power-law fluids over a flat plate under a magnetic field and pressure gradient, considering fluid injection and ejection. Hassanien et al. [2] and Tashtoush et al. [3] examined the heat transfer behavior of power-law fluids over a stretching surface with variable surface temperature, incorporating suction or injection effects. Sahu et al. [4] investigated the momentum and heat transfer in power-law fluids near a continuously moving plate, while Xu and Liao [5] examined heat transfer over a stretching flat sheet. Prasad and Vajravelu [6] analyzed magnetohydrodynamic (MHD) flow over a non-isothermal stretching sheet, extending the problem to include variable thermal conductivity and non-uniform heat generation [7]. Further studies have incorporated additional complexities, such as radiation and heat generation [8], slip velocity effects [9], non-linear stretching surfaces [10], and non-uniform heat generation [11]. Recent investigations have expanded into the effects of porosity on inclined plates [12] and unsteady electro-magnetohydrodynamic flows involving active and passive nanoparticle fluxes [13]. Alabdulaal et al. [14] reported that the power-law exponent exerts a favorable effect on heat transfer, but its influence on skin friction remains complex.

A recent innovation in heat transfer research involves the development of nanofluids containing nanoparticles made from highly conductive materials such as carbon, metals, and metal oxides. A more advanced class of nanofluids, known as nano-encapsulated phase change material (NEPCM) suspensions, incorporates phase change materials encapsulated within nanoparticles, thus providing an additional latent heat storage mechanism. Studies on NEPCM-based Newtonian nanofluids include Ghalambaz et al. [15], who investigated convection dynamics in NEPCM-water systems within enclosures, and Hajjar et al. [16], who analyzed NEPCM suspensions in periodically heated cavities. Other works, such as Alhashash and Saleh [17], examined heat transfer enhancement via enclosure rotation, while Wang et al. [18] explored entropy generation in localized NEPCM systems. Recently, Sheikholeslami et al. [19] proposed an enhancement methodology for photovoltaic systems, encompassing the integration of a nanofluid filter and a paraffin-based storage apparatus.

Despite these advances, the interaction of NEPCMs with power-law fluids remains largely unexplored, particularly under boundary-layer flow conditions. Only a few studies, such as Ghalambaz et al. [20] and Ali et al. [21], have considered NEPCM suspensions in non-Newtonian enclosures. However, to the best of the authors' knowledge, no investigation has addressed the hydrodynamic and thermal behavior of NEPCM-suspended power-law nanofluids over a stretching sheet with variable surface temperature.

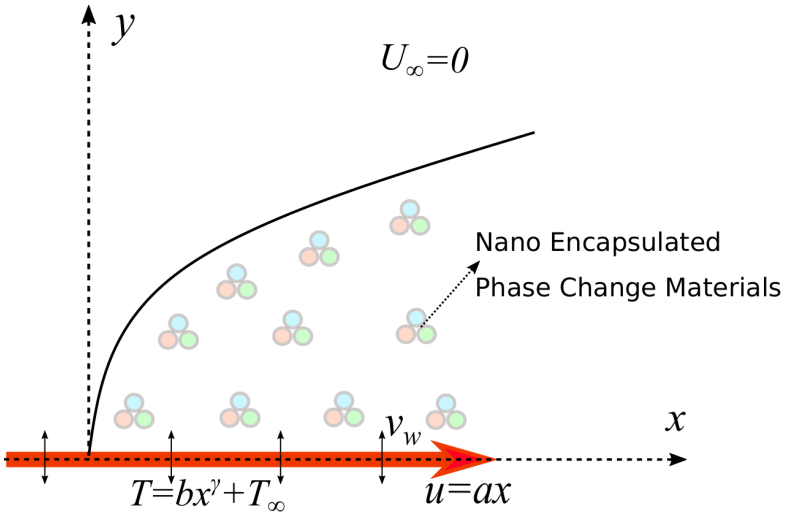

Figure 1: Schematic model of the flow over a stretching sheet contains NEPCMs suspended in the non-Newtonian base fluid.

The novelty of the present work lies in formulating and analyzing, for the first time, the boundary-layer flow and heat transfer of a power-law nanofluid embedded with NEPCMs over a non-isothermal stretching surface. The study provides a detailed parametric analysis of the effects of power-law index, NEPCM concentration, fusion temperature, and heating parameter on velocity, temperature, skin friction, and heat transfer rate. By coupling the rheological behavior of non-Newtonian fluids with the latent heat characteristics of NEPCMs, this research establishes a new framework for enhancing thermal transport in shear-dependent suspensions, with implications for advanced cooling, polymer processing, and energy storage applications.

2. Mathematical Formulation

Consider a two-dimensional, steady-state, incompressible boundary layer flow of a power-law nanofluid over a linearly stretching sheet. The x-axis is aligned with the flow direction, and the y-axis is normal to the surface. The sheet is stretched linearly, generating the flow as illustrated in Fig. 1. The fluid contains nano-encapsulated phase change materials (NEPCMs) suspended in a non-Newtonian base fluid. These NEPCMs absorb and release latent heat during phase transitions as they experience temperature variations within the boundary layer. The wall temperature distribution follows

$$T = bx^{\gamma} + T_w, \tag{1}$$

where T_w is the reference wall temperature, and γ is the power-law exponent describing the surface temperature variation. Using the boundary layer approximations, the governing equations are given as follows [22, 23]:

$$\frac{\partial u}{\partial x} + \frac{\partial v}{\partial y} = 0, \tag{2}$$

$$u\frac{\partial u}{\partial x} + v\frac{\partial u}{\partial y} = \nu_{nf}\frac{\partial}{\partial y}\left(\left|\frac{\partial u}{\partial y}\right|^{n-1}\frac{\partial u}{\partial y}\right), \tag{3}$$

$$u\frac{\partial T}{\partial x} + v\frac{\partial T}{\partial y} = \alpha_{nf}\frac{\partial^2 T}{\partial y^2}. \tag{4}$$

Equation (2) ensures mass conservation, while Eq. (3) represents the momentum balance in the boundary layer for a power-law fluid. Equation (4) governs the thermal energy transport, accounting for conduction and convection.

The corresponding boundary conditions are:

$$\begin{aligned} u = ax, \quad v = v_w(x), \quad T = bx^\gamma + T_w \quad \text{at} \quad y = 0, \\ u = 0, \quad T = T_\infty \quad \text{as} \quad y \to \infty. \end{aligned} \tag{5}$$

Here, u and v are the velocity components, a is the stretching rate, and $v_w(x)$ denotes the wall mass flux. The nanofluid's kinematic viscosity and effective thermal diffusivity are given by $\nu_{nf} = \mu_{nf}/\rho_{nf}$ and $\alpha_{nf} = k_{nf}/(\rho C_p)_{nf}$, respectively.

The effective density of the nanofluid is expressed as:

$$\rho_{nf} = (1-\phi)\rho_{bf} + \phi\rho_{ns}, \tag{6}$$

where ϕ is the nanoparticle volume fraction, and subscripts bf and ns denote the base fluid and NEPCM solid particles, respectively.

The NEPCM particle density is calculated as:

$$\rho_{Nm} = \frac{(1+\iota)\rho_{Nc}\rho_{Ns}}{\rho_{Ns} + \iota\rho_{Nc}}, \tag{7}$$

where ρ_{Nc} and ρ_{Ns} are the core and shell densities, and ι is the core-to-capsule mass ratio ($\iota \approx 0.447$ [24]).

The nanofluid's specific heat capacity is expressed as:

$$(C_p)_{nf} = \frac{(1-\phi)(\rho C_p)_{bf} + \phi(\rho C_p)_{Nm}}{\rho_{Nm}}. \tag{8}$$

This relation considers both the base fluid and the encapsulated nanoparticles.

To capture the phase change behavior, the specific heat of NEPCMs varies with temperature as:

$$C_{p,Nc} = C_{p,Nc,l} + \left[90^\circ\left(\frac{h_{sf}}{T_{Mr}} - C_{p,Nc,l}\right)\sin\left(180^\circ\frac{T - T_f + T_{Mr}/2}{T_{Mr}}\right)\right]\Gamma, \tag{9}$$

where T_{Mr} is the melting temperature range and Γ defines the active phase change region. This expression ensures smooth numerical convergence by representing latent heat effects through a sinusoidal model.

The effective thermal conductivity and viscosity properties of the suspension are:

$$k_{eff} = 1 + k_{Nm}\phi, \tag{10}$$

$$\mu_{eff} = 1 + \mu_{Nm}\phi. \tag{11}$$

Next, the similarity transformation is applied to reduce the governing PDEs into ODEs:

$$\psi = (\nu_{nf} a^{2n-1} x^{2n})^{1/(n+1)} f(\eta), \quad \Theta(\eta) = \frac{T - T_\infty}{T_w - T_\infty}, \quad \eta = \left(\frac{a^{2-n} x^{1-n}}{\nu_{nf}}\right)^{1/(n+1)} y. \tag{12}$$

Here, ψ is the stream function defined by $u = \frac{\partial \psi}{\partial y}$ and $v = -\frac{\partial \psi}{\partial x}$.

Substituting these transformations yields the following dimensionless equations:

$$\frac{(1 + \mu_{Nm}\phi)}{[(1-\phi) + \phi\rho_s/\rho_{bf}]} f'''(f'')^{n-1} + \frac{2n}{n+1} f f'' - (f')^2 = 0, \tag{13}$$

$$\frac{(1 + k_{Nm}\phi)}{C_r Pr} \Theta'' + \frac{2n}{n+1} f\Theta' - \gamma\Theta f' = 0. \tag{14}$$

Equation (13) governs the momentum transport of the non-Newtonian nanofluid, while Eq. (14) describes the corresponding energy transfer.

The boundary conditions are rewritten as:

$$\begin{aligned} f = 0, \quad f' = 1, \quad \Theta = 1 \quad \text{at} \quad \eta = 0, \\ f' = 0, \quad \Theta = 0 \quad \text{as} \quad \eta \to \infty. \end{aligned} \tag{15}$$

Finally, the key dimensionless performance measures are given as follows:

$$2C_f Re_x^{1/2} = (1 + \mu_{Nm}\phi)[f''(0)]^n, \tag{16}$$

$$Nu Re_x^{-1/2} = -(1 + k_{Nm}\phi)\Theta'(0). \tag{17}$$

Equations (16) and (17) represent the skin friction and local Nusselt number, respectively, providing insights into the shear and heat transfer performance along the stretching surface.

3. Computational Methodology

The coupled nonlinear boundary value problem (BVP) given by Eqs. (13)–(14), subject to the boundary conditions (15), was solved using the single–shooting method. This approach transforms the BVP into an equivalent initial value problem (IVP) whose unknown initial slopes are determined iteratively such that the far–field boundary conditions are satisfied [25].

The first step is to reduce the system to a first-order system. We then introduce the dependent variables:

$$y_1 = f, \quad y_2 = f', \quad y_3 = f'', \quad y_4 = \Theta, \quad y_5 = \Theta', \tag{18}$$

such that f''' and Θ'' can be obtained directly from the governing equations. Let

$$A = \frac{(1+\mu_{Nm}\phi)}{\left[(1-\phi)+\phi\frac{\rho_s}{\rho_{bf}}\right]}, \quad B = \frac{C_r Pr}{(1+k_{Nm}\phi)}. \tag{19}$$

From Eq. (13), the third derivative of f is expressed as

$$y_3' = f''' = \frac{y_2^2 - \frac{2n}{n+1} y_1 y_3}{A\, n\, (y_3)^{\,n-1}}. \tag{20}$$

Similarly, from Eq. (14), the second derivative of Θ is given by

$$y_5' = \Theta'' = B\left(\gamma\, y_4\, y_2 - \frac{2n}{n+1} y_1 y_5\right). \tag{21}$$

The complete first–order system becomes

$$y_1' = y_2, \tag{22}$$
$$y_2' = y_3, \tag{23}$$
$$y_3' = \frac{y_2^2 - \frac{2n}{n+1} y_1 y_3}{A\, n\, (y_3)^{\,n-1}}, \tag{24}$$
$$y_4' = y_5, \tag{25}$$
$$y_5' = B\left(\gamma\, y_4\, y_2 - \frac{2n}{n+1} y_1 y_5\right). \tag{26}$$

The boundary conditions at $\eta = 0$ are

$$y_1(0) = 0, \quad y_2(0) = 1, \quad y_4(0) = 1, \tag{27}$$

while $y_3(0) = \alpha$ and $y_5(0) = \beta$ are unknown initial slopes to be determined. At the far–field ($\eta \to \infty$), the requirements are

$$y_2(\infty) \to 0, \quad y_4(\infty) \to 0. \tag{28}$$

The shooting method treats α and β as free parameters and integrates Eqs. (22)–(26) from $\eta = 0$ to a sufficiently large $\eta_{\max}$, where the "infinity" conditions are approximated. The residual vector is defined as

$$\mathbf{R}(\alpha, \beta) = \begin{bmatrix} y_2(\eta_{\max}; \alpha, \beta) \\ y_4(\eta_{\max}; \alpha, \beta) \end{bmatrix}, \tag{29}$$

and the goal is to find (α, β) such that $\mathbf{R} \approx \mathbf{0}$.

The IVP above was integrated using the Runge–Kutta method. The far–field was truncated to $\eta_{\max}$ in the range $[4, 12]$ to ensure that $f'(\eta_{\max})$ and $\Theta(\eta_{\max})$ were sufficiently close to zero. The nonlinear system for (α, β) was solved using a Newton-type root-finding algorithm with Jacobian approximation. Convergence was declared when the infinity-norm of the residual vector was less than 0.000001. To avoid division by zero in Eq. (24) when $y_3 \to 0$, a small regularisation parameter ε was introduced, replacing $(y_3)^{n-1}$ by $(\max(|y_3|, \varepsilon))^{n-1}$ in the denominator. The choice $\varepsilon \approx 10^{-12}$ was found sufficient to maintain numerical stability without affecting accuracy. Additionally, parameter continuation was employed for challenging parameter regimes: solutions obtained for simpler cases (e.g., $n = 1$, $\gamma = 0$) were used as initial guesses for nearby parameter values.

To verify the accuracy of the numerical algorithm, we compared the present results with the benchmark solutions of Hassanien et al. [2] for the case of zero capsule volume fraction ($\phi = 0.0$). Table 1 reports the values of $f''(0)$ from the literature and the present computations together with the absolute and relative deviations. The absolute differences between the present results and Hassanien et al. are 3.0×10^{-5}, 2.0×10^{-5}, and 1.0×10^{-5} for $n = 0.3$, $n = 0.5$ and $n = 0.8$, respectively, which correspond to relative deviations of approximately 0.0020%, 0.0017% and 0.0010%. Such discrepancies are negligible and lie well within typical numerical round-off and truncation errors for boundary-layer similarity solutions. The small deviations can be attributed to minor differences in numerical implementation: (i) the finite truncation of the computational domain used to approximate the far-field boundary, (ii) tolerance criteria for the shooting/Newton iterations, and (iii) interpolation/rounding conventions when reporting tabulated results.

Table 1: The values $f''(0)$ in comparison to results from the literature.

n	Present work	[2]
0.3	1.48680	1.48677
0.5	1.16526	1.16524
0.8	1.02884	1.02883

Currently, no experimental data are available for the specific configuration of a power-law fluid containing NEPCM capsules over a non-isothermal stretching sheet; hence, direct experimental validation is not feasible. Nevertheless, the benchmark comparison confirms the accuracy of the hydrodynamic solver for the limiting case $\phi = 0$. The NEPCM-augmented model adopts constitutive and latent-heat formulations consistent with recent literature, though its underlying assumptions (e.g., single-phase approximation, capsule homogeneity) require future experimental verification. Accordingly, experimental validation is recommended as a priority for subsequent investigations.

4. Results and Discussion

Subsequent numerical analyses are conducted using dimensionless variables across the defined parameter ranges: NEPCM volume fraction ($0.0 \leq \phi \leq 0.05$), power-law index ($0 \leq n \leq 0.9$), fusion temperature ($0.1 \leq \Theta_f \leq 0.3$), and heating parameter ($-1 \leq \gamma \leq 1$). The Prandtl and Stefan numbers are fixed at $Pr = 6.2$ and $Ste = 0.2$, respectively.

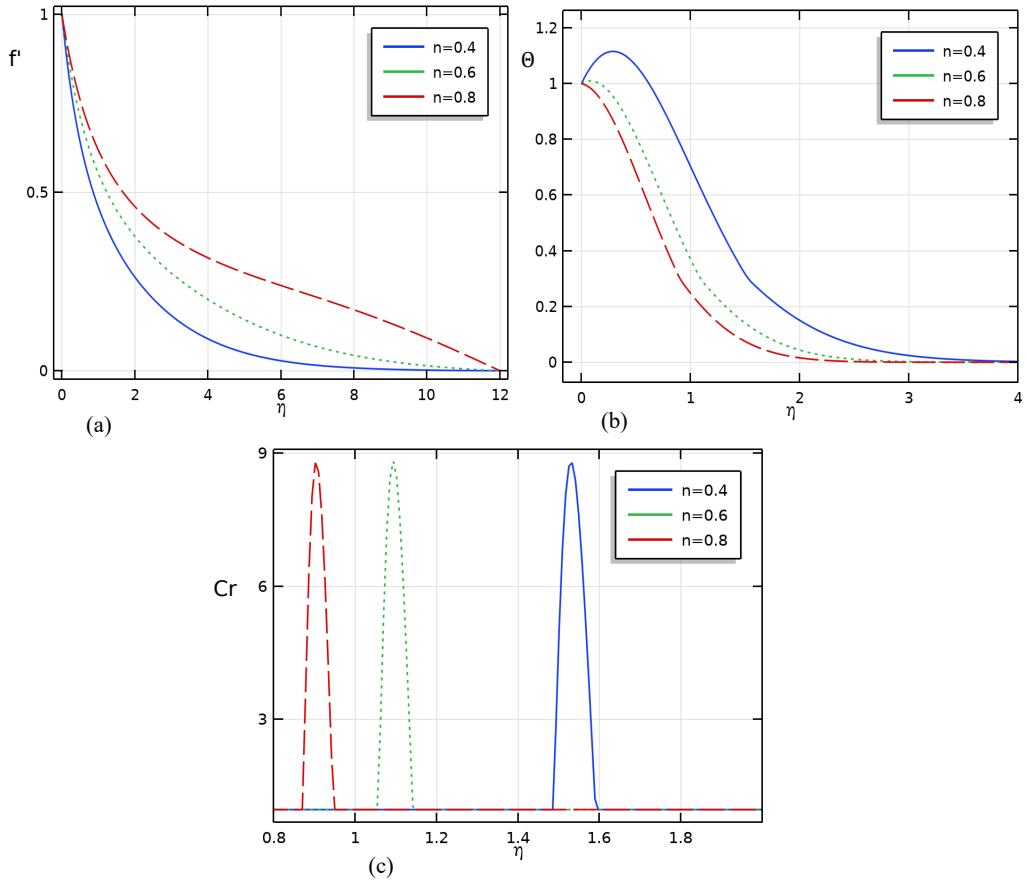

Figure 2: Impact of the power-law index on velocity (a), temperature (b) and heat capacity profile (c) at $\phi = 0.05$, $\Theta_f = 0.3$, $Ste = 0.2$ and $\gamma = -1$.

Figure 2 shows the evolution of the velocity (a), temperature (b) and heat capacity profile (c) by varying the power-law index at $\phi = 0.05$, $\Theta_f = 0.3$, and $\gamma = -1$. The velocity decreases markedly as n increases, indicating enhanced viscous resistance within the boundary layer. This trend reflects the dominance of pseudoplastic (shear-thinning) behavior for $n < 1$, where effective viscosity increases with reduced shear rate. For reference, the opposite trend would occur in a shear-thickening fluid ($n > 1$). The observed suppression of velocity with increasing n demonstrates the rheological control of momentum transport.

The temperature field shows a reduction with higher n, due to weakened convective motion and diminished thermal diffusion. At lower n values, thermal penetration is stronger, occasionally producing temperature overshoots near the plate—an outcome of more efficient energy redistribution in shear-thinning fluids. The corresponding shift of the heat capacity ratio profile toward the surface at larger n implies greater local energy storage in the near-wall region, consistent with enhanced viscous heating resistance. In practical terms, this behavior is crucial for non-Newtonian materials processing such as polymer extrusion and coating flows, where optimizing the rheological index allows regulation of both heat distribution and wall shear, thereby improving product uniformity and preventing overheating in viscous materials.

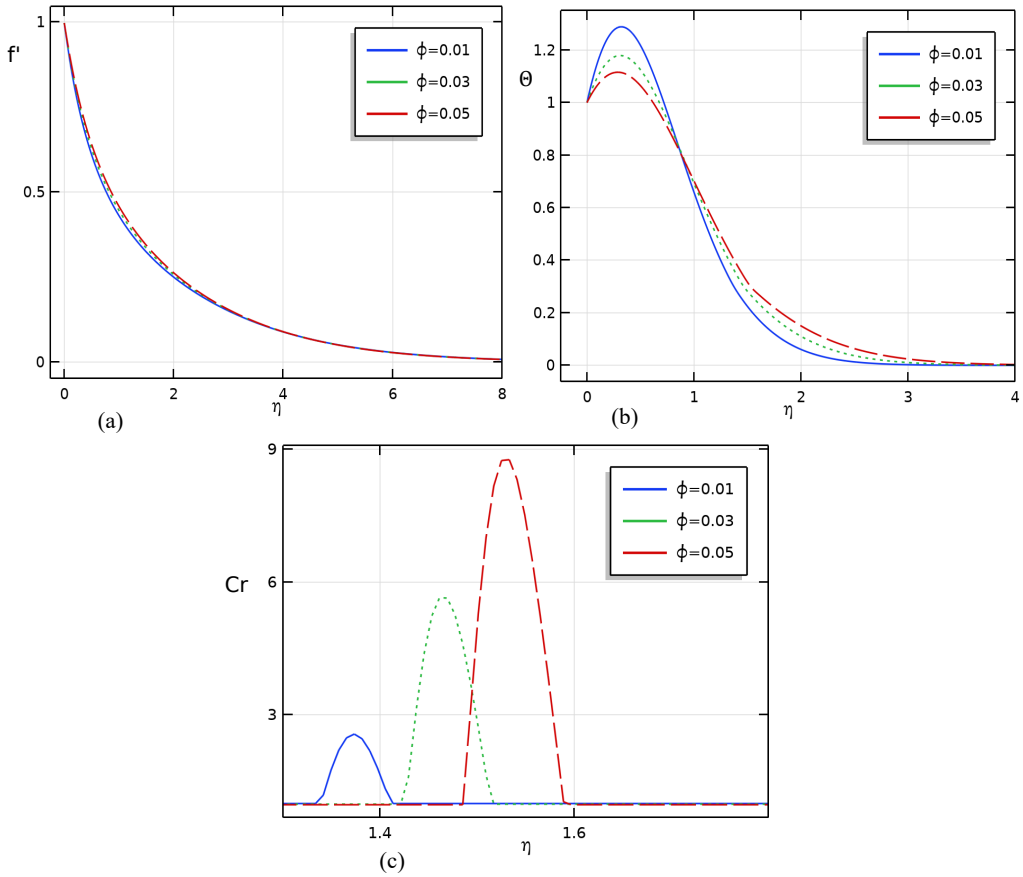

Figure 3: Impact of the nano encapsulated PCM concentration on velocity (a), temperature (b) and heat capacity profile (c) at $n = 0.4$, $\Theta_f = 0.3$, and $\gamma = -1$.

Figure 3 shows the evolution of the velocity (a), temperature (b) and heat capacity profile (c) by varying NEPCMs concentration at $n = 0.4$, $\Theta_f = 0.3$, and $\gamma = -1$. Increasing ϕ slightly elevates the fluid velocity, attributed to buoyancy-assisted momentum transfer from encapsulated particles. More notably, the temperature profile rises substan-

tially with higher NEPCM content, demonstrating the ability of the capsules to absorb and release latent heat during phase transition. The thermal boundary layer expands, enhancing heat storage and delaying thermal decay away from the wall.

The observed behavior aligns with experimental and numerical studies such as Adel et al. [26], where NEPCM addition improved energy buffering capacity. The broadening of the heat capacity ratio profile reflects more distributed heat absorption across the boundary layer. From an engineering perspective, increasing NEPCM concentration is beneficial for systems requiring temperature stabilization, such as in electronics cooling, thermal regulation of solar collectors, or battery thermal management where latent heat buffering mitigates temperature fluctuations under variable loads as reported by Sheikholeslami [27].

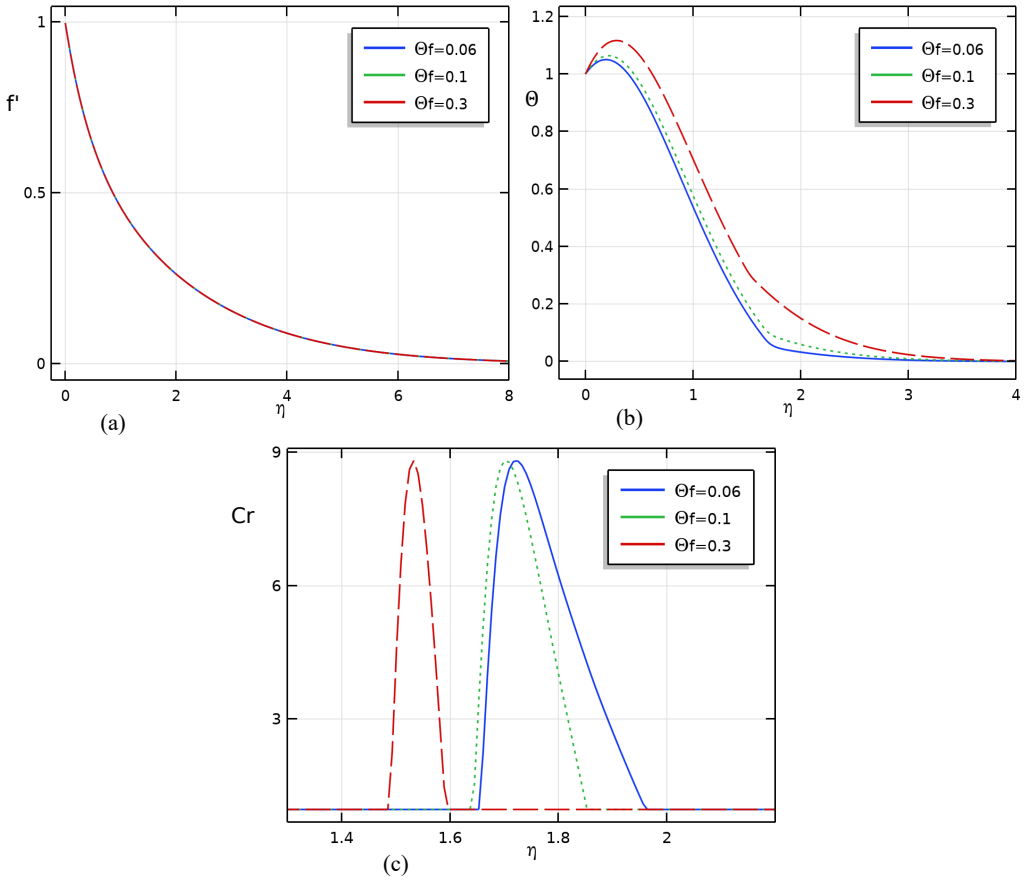

Figure 4: Impact of the fusion temperature on velocity (a), temperature (b) and heat capacity profile (c) at $n = 0.4$, $\phi = 0.05$, and $\gamma = -1$.

Figure 4 shows the evolution of the velocity (a), temperature (b) and heat capacity profile (c) by varying fusion temperature at $n = 0.4$, $\phi = 0.05$, and $\gamma = -1$. The velocity remains essentially unchanged with variations in Θ_f, confirming that hydrodynamics are

dominated by rheology rather than thermal phase behavior. However, temperature and heat capacity ratio increase significantly with higher fusion temperature, as higher Θ_f delays melting and promotes greater latent heat release near the wall region. The shift of the heat capacity ratio curve toward the surface indicates localized energy storage, while its compression suggests a narrower effective melting zone. These behaviors are critical in applications such as heat exchangers or thermal energy storage tanks, where tuning the PCM fusion temperature can optimize the thermal response for specific operating ranges.

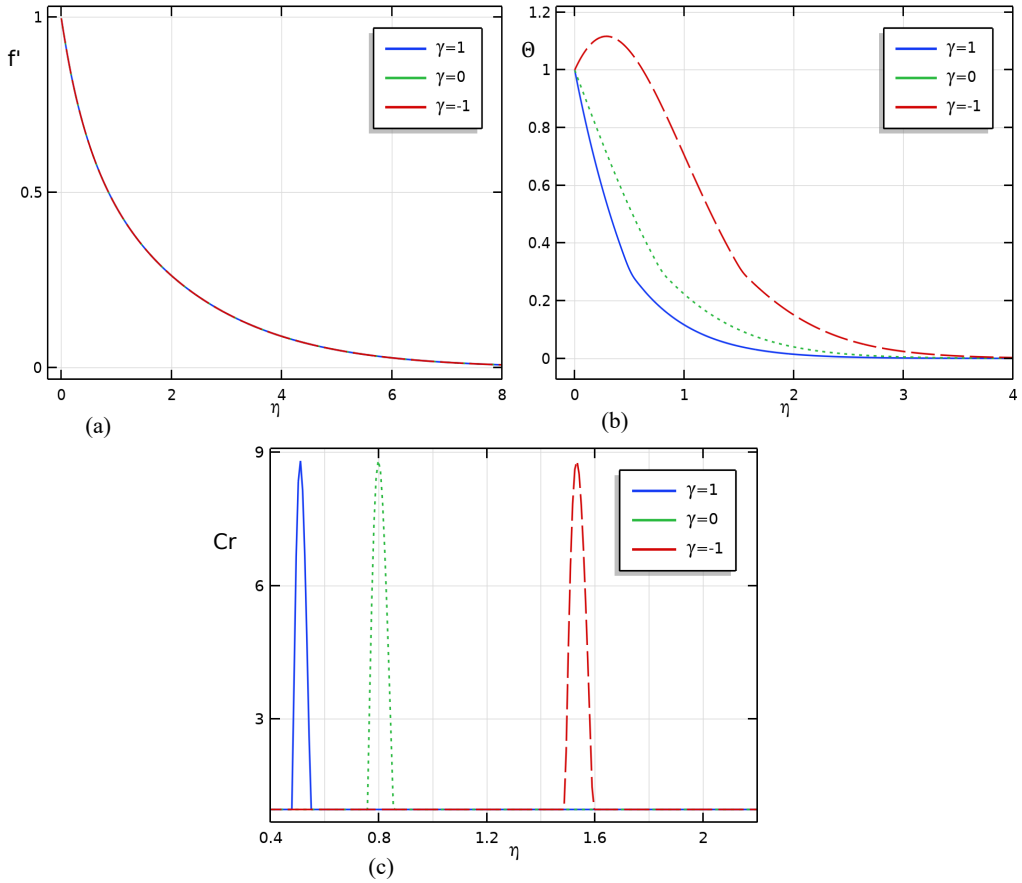

Figure 5: Impact of the temperature parameter on velocity (a), temperature (b) and heat capacity ratio (c) at $n = 0.4$, $\phi = 0.05$, and $\Theta_f = 0.3$.

Figure 5 shows the evolution of the velocity (a), temperature (b) and heat capacity ratio (c) by varying temperature parameter at $n = 0.4$, $\phi = 0.05$, and $\Theta_f = 0.3$. The velocity profile remains almost unaffected by γ, underscoring the hydrodynamic robustness of power-law fluids under thermal perturbations. However, the temperature decreases under positive γ (heating) due to enhanced heat removal, while negative γ (cooling) leads to greater thermal accumulation.

The proximity of the heat capacity ratio profile to the plate at higher γ indicates

that energy storage becomes concentrated near the surface during heating. The decoupling between velocity and temperature responses implies that, in practical devices such as polymer-film stretchers or cooling channels, thermal performance can be controlled via surface heating conditions without disturbing flow stability—a desirable feature for precision manufacturing and thermal regulation systems.

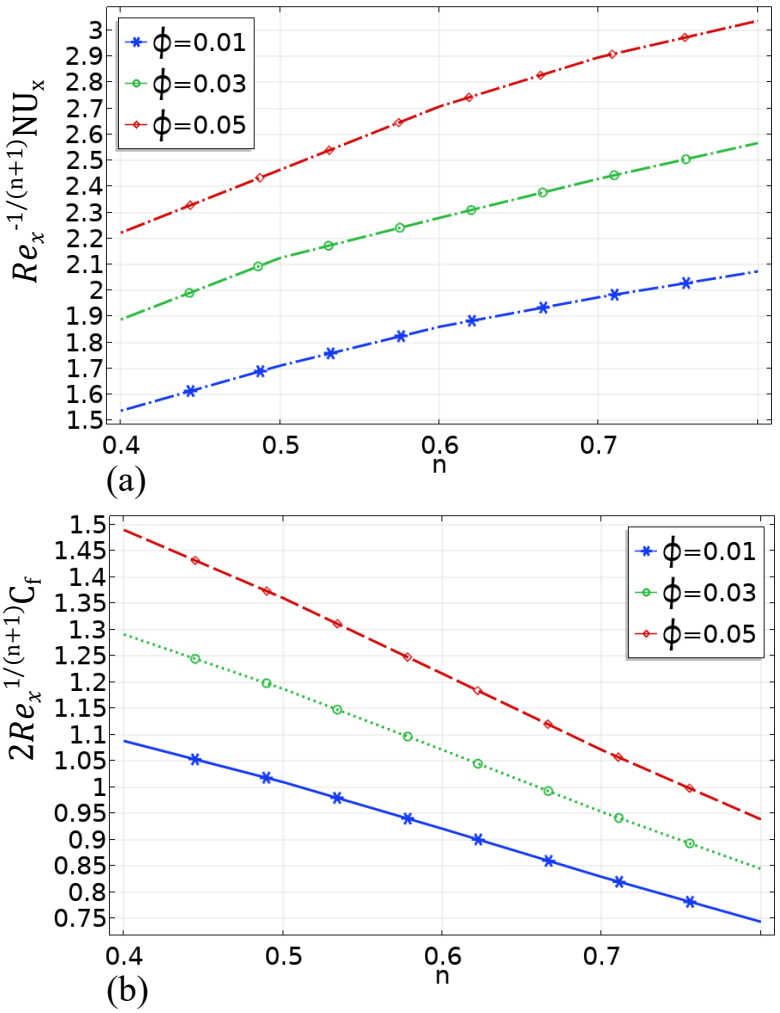

Figure 6: Impacts of the NEPCMs volume fraction on the Nusselt number (a) and the skin friction coefficient (b) versus the power law index for $\Theta_f = 0.3$, $\gamma = 0.0$.

Figures 6–8 present the combined influence of NEPCM concentration, power-law index, fusion temperature, and heating parameter on the Nusselt number and skin friction coefficient. In Figure 6, increasing NEPCM concentration enhances the Nusselt number due to the latent heat contribution of encapsulated particles, while higher n values (shear-thinning behavior) promote a modest additional increase by improving thermal boundary layer structure. Conversely, skin friction rises with NEPCM concentration but decreases

with n, illustrating a competition between viscous thickening by particle addition and viscosity reduction through shear-thinning. The decline in skin friction from $n = 0.4$ to $n = 0.7$ suggests that the rheological effect dominates over the particle-induced drag enhancement.

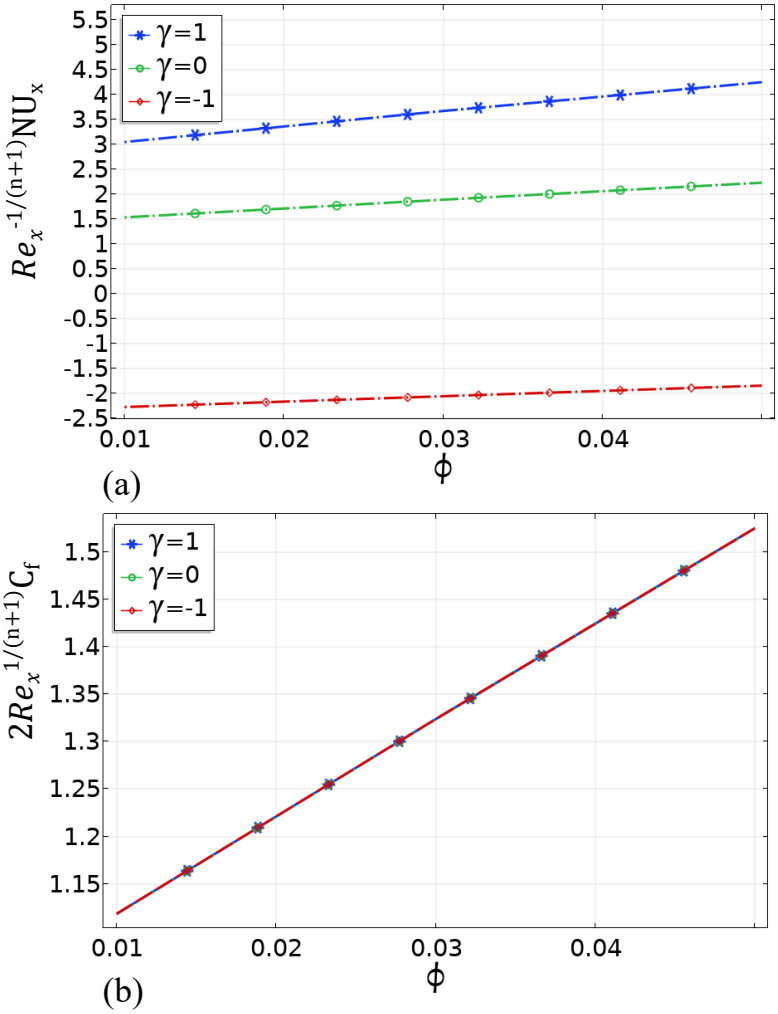

Figure 7: Impacts of the heating parameter on the Nusselt number (a) and the skin friction coefficient (b) versus the power law index for $\Theta_f = 0.3$, $n = 0.4$.

Figure 7 shows the effect of heating parameter on the local Nusselt number (a) and the skin friction coefficient (b) with respect to the power law index $\Theta_f = 0.3$, $n = 0.4$. It shows that heating parameter γ primarily affects heat transfer while leaving skin friction nearly unchanged, highlighting that thermal boundary manipulation alters energy transport without destabilizing flow, a feature desirable for thermally controlled surface processes.

Figure 8 shows how fusion temperature affects (a) the local Nusselt number and (b) the

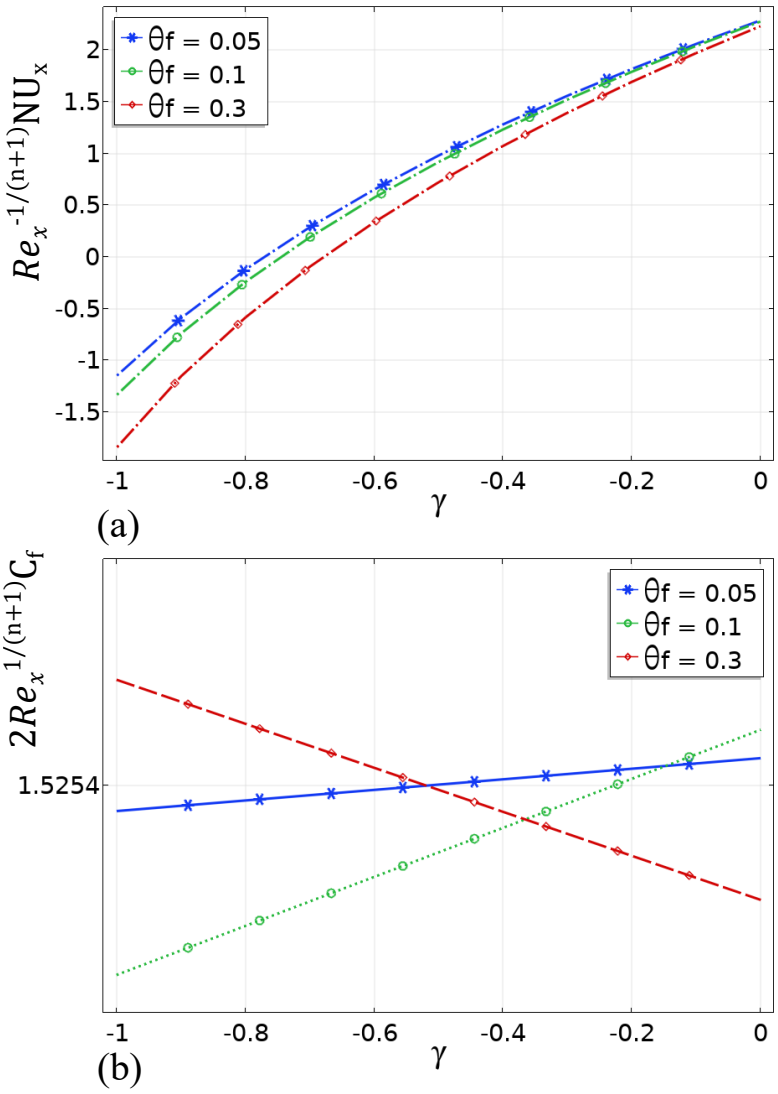

Figure 8: Impacts of the fusion temperature on the Nusselt number (a) and the skin friction coefficient (b) versus the heating parameter for $\phi = 0.05$, $n = 0.4$.

skin friction coefficient, when the power-law index is held constant at $n = 0.4$ and $\phi = 0.05$. It reveals that higher fusion temperatures reduce the Nusselt number because phase change occurs less readily, limiting latent heat utilization. The interplay between γ and Θ_f also shows that excessive heating can counteract PCM storage benefits, underscoring the need for optimized material selection. This insight is valuable for the design of NEPCM-enhanced heat exchangers or microchannel coolers, where selecting the proper PCM fusion temperature is crucial to achieving efficient heat dissipation under varying operational loads.

5. Conclusions

This study investigated the hydrodynamic and thermal behavior of power-law nanofluids embedded with nano-encapsulated phase change materials (NEPCMs) over a non-isothermal stretching sheet. The governing boundary-layer equations were transformed into similarity form and solved numerically using the shooting method combined with Runge–Kutta integration and Newton iteration. The results revealed that increasing the power-law index markedly reduces the fluid velocity and suppresses the temperature distribution, indicating that shear-thickening behavior enhances viscous resistance and significantly influences the flow dynamics. Furthermore, higher NEPCM concentrations were found to thicken the thermal boundary layer and elevate the heat capacity ratio, thereby improving the overall heat transfer performance, as evidenced by the increase in Nusselt numbers.

The study also demonstrated that the fusion temperature and the heating parameter strongly affect the thermal field and heat storage capacity, while exerting a negligible impact on velocity profiles. This finding suggests a decoupling between the hydrodynamic and thermodynamic behaviors of NEPCM-based power-law fluids. Additionally, it was observed that the inclusion of NEPCMs enhances heat transfer but simultaneously increases wall shear stress. However, this effect is mitigated at higher power-law indices, indicating a competitive interaction between the rheological characteristics of the base fluid and the concentration of NEPCMs.

Overall, this work provides new insights into the coupled rheological and thermal mechanisms governing NEPCM-laden non-Newtonian fluids. The findings contribute to the understanding of complex heat transfer processes in shear-dependent suspensions and are expected to inform the design and optimization of advanced thermal management systems. Potential applications include energy storage units, polymer extrusion processes, and high-performance cooling systems, where improved heat transfer is required without compromising flow stability. Future research could extend the present analysis to unsteady, three-dimensional, and magnetohydrodynamic configurations to broaden the applicability of NEPCM-based non-Newtonian suspensions in industrial and energy-related technologies.

Data Availability

The data that support the result of this study are available upon request from the authors.

Conflict of Interests

The author declares that there is no competing of interests in publishing this article.

Acknowledgements

This research was funded by Daftar Isian Pelaksanaan Anggaran (DIPA) Universitas Riau Nomor SP DIPA-139.03.2.693425/2025 Date 02 December 2024.

References

[1] MH Cobble. Magnetohydrodynamic flow for a non-newtonian power-law fluid having a pressure gradient and fluid injection. *Journal of Engineering Mathematics*, 14(1):47–55, 1980.

[2] I.A. Hassanien, A.A. Abdullah, and R.S.R. Gorla. Flow and heat transfer in a power-law fluid over a nonisothermal stretching sheet. *Mathematical and computer modelling*, 28(9):105–116, 1998.

[3] B. Tashtoush, Z. Kodah, and A. Al-Ghasem. On thermal boundary layer of a non-Newtonian fluid on a power-law stretched surface of variable temperature with suction or injection. *Heat Mass Transf.*, 37(4):459–465, 2001.

[4] A.K. Sahu, M.N. Mathur, P. Chaturani, and S.S. Bharatiya. Momentum and heat transfer from a continuous moving surface to a power-law fluid. *Acta Mech.*, 142(1):119–131, 2000.

[5] H. Xu and S.J. Liao. Laminar flow and heat transfer in the boundary-layer of non-Newtonian fluids over a stretching flat sheet. *Comput. Math. Appl.*, 57(9):1425–1431, 2009.

[6] K.V. Prasad and K. Vajravelu. Heat transfer in the MHD flow of a power law fluid over a non-isothermal stretching sheet. *Int. J. Heat Mass Transf.*, 52(21-22):4956–4965, 2009.

[7] M.S. Abel, P.S. Datti, and N. Mahesha. Flow and heat transfer in a power-law fluid over a stretching sheet with variable thermal conductivity and non-uniform heat source. *Int. J. Heat Mass Transf.*, 52(11-12):2902–2913, 2009.

[8] C.H. Chen. Magneto-hydrodynamic mixed convection of a power-law fluid past a stretching surface in the presence of thermal radiation and internal heat generation/absorption. *International Journal of Non-Linear Mechanics*, 44(6):596–603, 2009.

[9] M.A.A. Mahmoud. Slip velocity effect on a non-Newtonian power-law fluid over a moving permeable surface with heat generation. *Mathematical and Computer Modelling*, 54(5-6):1228–1237, 2011.

[10] A.M. Megahed. Flow and heat transfer of a non-newtonian power-law fluid over a non-linearly stretching vertical surface with heat flux and thermal radiation. *Meccanica*, 50(7):1693–1700, 2015.

[11] S.R. Mishra, S. Baag, G.C. Dash, and M.R. Acharya. Numerical approach to mhd flow of power-law fluid on a stretching sheet with non-uniform heat source. *Nonlinear Engineering*, 9(1):81–93, 2019.

[12] G. Revathi, G. Veeram, M.J. Babu, K.S. Babu, and K.A. Suneel. Darcy–Forchheimer flow of power-law (Ostwald-de Waele type) nanofluid over an inclined plate with

thermal radiation and activation energy: an irreversibility analysis. *Int. J. Ambient Energy*, 44(1):1980–1989, 2023.

[13] S. Chandel, S. Sood, S. Sharma, and S. Prasad. Unsteady power law nanofluid flow subjected to electro-magnetohydrodynamics with active and passive nanoparticles flux. *Journal of Nanofluids*, 12(8):2078–2091, 2023.

[14] T.H. AlAbdulaal, S. Rehman, H. Ali, U. Riaz, and S. Znaidia. Exploring slip flow and heat transfer of power-law fluid past an induced magnetic stretching regime subject to Cattaneo-Christov flux theory. *Case Stud. Therm. Eng.*, page 105325, 2024.

[15] M. Ghalambaz, A.J. Chamkha, and D. Wen. Natural convective flow and heat transfer of nano-encapsulated phase change materials (NEPCMs) in a cavity. *Int. J. Heat Mass Transf.*, 138:738–749, 2019.

[16] A. Hajjar, S.A.M. Mehryan, and M. Ghalambaz. Time periodic natural convection heat transfer in a nano-encapsulated phase-change suspension. *Int. J. Mechanical Sci.*, 166:105243, 2020.

[17] A. Alhashash and H. Saleh. Free convection flow of a heterogeneous mixture of water and nano-encapsulated phase change particle (NEPCP) in enclosure subject to rotation. *J. Energy Storage*, 51:104168, 2022.

[18] W. Wang, Y.H. Jin, Y.M. Chen, Z.M. Hu, R.R. Zhou, H. Tian, F. Xin, and X.Z. Li. Hydrothermal and entropy generation analyses of natural convection of nano-encapsulated phase change materials suspension in a cavity subjected to the localized heating. *J. Energy Storage*, 77:109865, 2024.

[19] M. Sheikholeslami, Z. Khalili, F. Salehi, and L. Momayez. Simulation of sustainable solar thermal storage system involving photovoltaic panel equipped with nanofluid-based splitter considering self-cleaning coating. *Sustainable Cities and Society*, 119:106100, 2025.

[20] M. Ghalambaz, K.A. Ayoubloo, and A. Hajjar. Melting heat transfer of a non-Newtonian phase change material in a cylindrical vertical-cavity partially filled porous media. *Int. J. Numer. Meth. Heat Fluid Flow*, 30:3765–3789, 2020.

[21] F.H. Ali, H.K. Hamzah, S.Y. Ahmed, M.A. Ismael, Z. Haddad, M. Ghalambaz, A.M. Abed, K. Al-Farhany, W. Jamshed, and M.R. Eid. Convective heat transference of non-Newtonian functional phase variation nano-encapsulated liquids. *Int. J. Mod. Phys. B*, 37(29):2350258, 2023.

[22] K. Vajravelu, K.V. Prasad, and C.N. Ng. Unsteady flow and heat transfer in a thin film of Ostwald–de Waele liquid over a stretching surface. *Communications in Nonlinear Science and Numerical Simulation*, 17(11):4163–4173, 2012.

[23] A.S. Dogonchi, N.S. Bondareva, M.A. Sheremet, S. El-Sapa, A.J. Chamkha, and N.A. Shah. Entropy generation and heat transfer performance analysis of a non-Newtonian NEPCM in an inclined chamber with complicated heater inside. *J. Energy Storage*, 72:108745, 2023.

[24] S. Barlak, O.M. Sara, A. Karaipekli, and S. Yapıcı. Thermal conductivity and viscosity of nanofluids having nanoencapsulated phase change material. *Nanosc. Microsc Therm.*, 20(2):85–96, 2016.

[25] L. Deswita and H. Saleh. Effect of nano-encapsulated phase change materials on

Blasius and Sakiadis flow. *Int. Comm. Heat Mass Transf.*, 159:108225, 2024.

[26] M. Adel, M.M. Khader, M.M. Babatin, I. Alraddadi, A. Alaidrous, and G.M. Ismail. Heat transfer and magnetohydrodynamic nanofluid flow caused by a stretching sheet heated convectively: Numerical investigation. *Eur. J. Pure Appl.*, 18(1):5502–5502, 2025.

[27] M. Sheikholeslami. Numerical analysis of solar energy storage within a double pipe utilizing nanoparticles for expedition of melting. *Solar Energy Materials and Solar Cells*, 245:111856, 2022.